Robust Heart Rate Monitoring by a Single Wrist-Worn Accelerometer Based on Signal Decomposition

Chao Zhao, Wenru Zeng, Dandan Hu, and Hong Liu

***Abstract*—Monitoring heart rate (HR) by a single wrist-worn accelerometer would provide many advantages over electrocardiogram (ECG) or photoplethysmography (PPG), such as wearing comfortability, saving power, tiny footprint and automatic motion artifact removal. However, like ECG, accelerometry was mostly implemented on the chest, named seismocardiogram (SCG), and PPG was dominating the wrist worn format. Pulse condition detection in Traditional Chinese Medicine or sphygmography was engineered into a wearable format in this work, and a wrist-worn HR monitor by a single accelerometer was demonstrated. A major limitation of wrist-worn device is that motion artifacts and noise severely corrupt the signal integrity. In this study, with raw data segments including hundreds of random finger or hand motions, several signal decomposition algorithms were compared, such as independent component analysis (ICA), variable mode decomposition (VMD), wavelet synchrosqueezed transform (WSST), and singular spectrum analysis (SSA), and Kalman smoothing was implemented to track HR continuously. Our method was tested on 20 subjects during random finger tapping or hand swinging. Without knowing properties of noise or motion beforehand or requirement of an extra sensor as reference, our method provides a significant removal of motion artifacts and noise from three-dimensional acceleration signals, with 95% of HR estimation within ±8.86 bpm, much longer battery life and better wearing comfort than PPG. It would broaden the working conditions, and thus provide a more holistic assessment of HR during everyday life.**

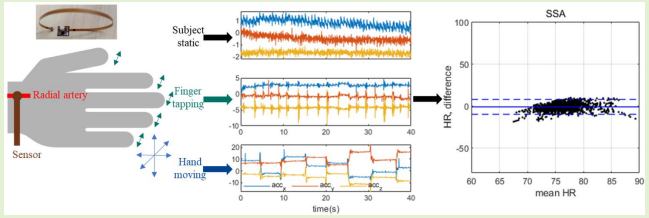

***Index Terms*— Accelerometers, heart rate, motion artifacts, singular spectrum analysis, Kalman smoothing, wearable sensors.**

I. Introduction

CONTINUOUS monitoring of vital cardiovascular signals like HR, is beneficial for both healthy individual and person with cardiac diseases [1], to promote active and healthy lifestyle and detect heart disease for early stage preventions. It finds applications during aerobic exercise, obstructive sleep apnea monitoring or other scenarios, and can help to detect atrial fibrillation, arrhythmia, heart attack and evaluate stress and psychological health [2], etc. Especially considering the aging population, prevalence of cardiovascular diseases, outbreaks of infectious diseases affecting cardiovascular systems and short-handed healthcare professionals, a wearable and multifunctional monitor which could provide continuous, seamless, pervasive and accurate detection of heart rate in ambulatory settings or at home is critical, and serves as a cornerstone in mobile health informatics.

For heart rate monitoring, ECG is de facto gold standard in clinics, whereas its multiple electrodes with gel make it obtrusive and cumbersome for everyday usage. Wearable ECG needs the user to wear it on one hand, and touch the ECG electrode with another hand to complete the circuit connection, while preventing the continuous measurement of HR [3]. PPG is the most popular technology for HR monitoring in consumer markets and in the literature [4]–[6]. Due to the high-power consumption (typically hundreds higher than accelerometer), extra 3.3V power supply for LED, large footprint (typically ten times larger than accelerometer) and light intensity drifting of LED in long term usage, most of the commercial or research-purpose PPG device only measure intermittent heart rate every tens of seconds to even one minute, which may miss the critical heart rate transition point. With motion artifact in everyday usage, its accuracy couldn't meet clinical requirement, due to ambient light leakage, contact-pressure variations and change in blood flow [7], [8]. Usually, an accelerometer is

Manuscript received March 22, 2021; revised April 20, 2021; accepted April 21, 2021. Date of publication April 23, 2021; date of current version July 14, 2021. This work was supported in part by the National Natural Science Foundation of China under Grant 21635001, in part by the State Key Project of Research and Development under Grant 2016YFF0100802, and in part by the Key Project and Open Research Fund of State Key Laboratory of Bioelectronics, Southeast University. The associate editor coordinating the review of this article and approving it for publication was Dr. Cheng-Sheng Huang. *(Corresponding author: Hong Liu.)*

The authors are with the State Key Laboratory of Bioelectronics, School of Biological Science and Medical Engineering, Southeast University, Nanjing 210096, China (e-mail: liuh@seu.edu.cn).

Digital Object Identifier 10.1109/JSEN.2021.3075109

accompanied to partially remove the artifact, whose types are severely limited by underlying algorithm and often requires a sharp difference in amplitude, frequency or waveform between heart beat and motion artifacts. PPG is also accompanied with impedance plethysmography (IPG) or ECG/PPG for further waveform extraction and more accurate measurement for medical grade applications [3], [9], [10].

Besides optical or electrical detection, visual heart vibration, named SCG could provide the mechanical outcomes of myocardial activity, valve motions and others that are absent from ECG or PPG signals, in which accelerometry is the dominating technology. Although accelerometry was typically used in posture and movement classification, energy expenditure estimation, fall detection and balance control evaluation [11], [12], along with the integration and minimization of state-of-the-art MEMS and CMOS technology, accelerometer with higher sensitivity, lower power consumption and tiny footprint was designed and fabricated for sensing subtle human body micromotion aimed at physiological monitoring and clinical applications, such as heart rate or cardiovascular profile monitoring. Accelerometers in the current literature about SCG are embedded in a rigid printed circuit board with other components which make them unsensitive and unwearable for curved skin on body such as the wrist, and their full potential to detect ultra subtle micromotion on the human body is not realized yet. Also, the requirement of attaching accelerometer on the chest for minimizing motion artifacts and boosting signal to noise ratio limits SCG's working conditions. Besides accelerometry, strain gauge on radial [13], carotid [14], or superficial temporal artery [15] termed sphygmography analyzing pulse waveform to derive the heart rate also attracts lots of attention in the community. Flexible piezoelectric film in sphygmography or other novel materials shows high sensitivity and high responding frequency, but they suffer from signal drifting, performance degradation, and 1D respondence without self-calibration capability [16], [17]. From the aspect of a wrist-worn hardware, a minimized accelerometer on flexible PCB combines the advantages of SCG and sphygmography for ambulatory settings or home usage. Thus, in this study, wearable HR monitoring by a high sensitivity ($\sim 2\ \mu N$), small footprint ($\sim 8\ mm^2$), light-weight (29 mg), and flexible accelerometry system was demonstrated. Because of the advantage of hardware design and fabrication, it could be attached to many skin areas for HR monitoring.

The signal to noise ratio and data quality is compromised when the accelerometer is worn on the wrist, and efficiency of heart rate detection algorithm categorized into adaptive filtering, spectral filtering, learning-based methods or signal decomposition are highly coupled with the underlying hardware, firmware and types of motion artifacts. In the literature, analysis of heart rate or other physiological signals implementing accelerometry with motion artifact was followed by Hilbert transform [18], Hidden Markov Model [19], variational mode decomposition [20], multiscale wavelet decomposition [21], logistic regression [22], spectral entropy and heart rate variability [23], 3D trajectory [24], short time Fourier transform [25], adaptive line enhancer and singular spectrum [26], RobustICA [27], supporting vector machines [28], multi-objective hierarchical classification [29], or other novel algorithms for signal processing to derive HR. Motion artifact analyzed or removed by filtering in the literature are commonly in a different frequency from the desired physiological signal [30], while the two frequency ranges usually are overlapped and heart rate could be severely corrupted by finger or hand motion [31]. Root mean squared (RMS) filter was commonly used by setting a threshold of the signal amplitude, which requires a sharp magnitude difference between motion artifact and heart beating signals. Also, several filtering methods requires another sensor as reference, and lies on the hypothesis of linear relationship between clean signal and noise. Besides adaptive filtering or spectrum filtering, advanced learning-based methods typically require preprocessing and training to get a template of clean heart beat and various motions. Templates could be firstly generated by dictionary learning, and XGBoost [32] was implemented to recognize motion by orthogonal matching pursuit (OMP) [33]. Other template matching algorithm, such as modified time-frequency matching pursuit (TFMP), could be utilized to recognize and remove motion artifacts. Also, dynamic-time feature matching (DTFM), modified from dynamic time warping (DTW), was utilized to find the correlation between templates and raw signal for further evaluation [34]. These learning-based methods need to generate templates beforehand for regulated motions like walking, running or jogging etc., while most of motion artifacts were random and unpredictable, and often for new object or new motions, the model needed to be retrained.

Signal decomposition provides another category of algorithms for artifact and noise removal. It could decompose the raw signal into several components, select the most needed and reconstruct the signal. It needs no reference sensor, weak requirement of frequency or magnitude difference between signal and noise, and no overcomplete training datasets. In this work, four widely used and popular signal decomposition methods, ICA, VMD, WSST and SSA were implemented and compared. ICA is a tool for blind source separation (BSS) aiming at decomposing an observed random vector into statistically independent variables [35]. It can deal with a general mixing structure, opposed to classical principal component analysis (PCA) which can only process orthogonal columns, but is limited by the assumption of statistical independence. VMD is widely used to concurrently decompose a signal into different modes of unknown but separate spectral bands [36]. It is much more robust to sampling and noise, compared to classic empirical mode decomposition (EMD). WSST is a time-frequency signal analysis algorithm to decompose signals into constituent components with time-varying oscillatory characteristics [37]. It is robust to bounded perturbations of the signal and to Gaussian white noise, and has superior precision in both time and frequency [38]. However, both VMD and WSST results are contaminated by noise at the same frequency bands of the signal, and a few parameters need to be set beforehand. SSA is a useful tool to decompose the original series into the sum of several independent and interpretable components such as a slowly varying trend, oscillatory components and a structureless noise, depending on a preset threshold [39]. Nevertheless, ICA and SSA require more

than one sensor, and usually are applied on an array of sensors or two different types of sensors (e.g. PPG and accelerometer). Previously, the correlation of 3 axis signals were not fully explored, usually with a principle axis chosen and other axis signals simply dumped. Here SSA was implemented on 3D signals and outperformed other decomposition methods. Raw HR estimates were calculated from the reconstructed heart beating signals. Furthermore, a Kalman smoothing algorithm is implemented to remove outliers and convert a continuous time series of HR to interpolated estimates [40], [41].

Overall, our work presents a single wrist-worn accelerometer for continuous HR monitoring with simultaneous motion artifacts and noise removal, while most of earlier works utilizing PPG to track HR need another accelerometer to remove motion artifacts. By adopting an alternatively mechanic HR monitoring method compared to the popular optical one, it consumed about 1000 times smaller power for continuous HR monitoring and required several times smaller footprint. Thus, it has a much longer battery life and better wearing comfort for more application scenarios and better user satisfactory. The rest of this paper is organized as follows: Section II will present the device and accompanying algorithms for HR monitoring. Section III will present the performance of our system when different motion artifacts from finger or hand moving were corrupting the HR signal. Section IV will discuss our method's advantages and limitations, and conclude the paper with promising directions for future research. Section V is the conclusion of our methods.

II. Materials and Methods

A. Apparatus and Experimental Protocol

The block diagram of the wearable prototype is shown in Fig. 1. The mCube MC3672 with a 1.3 mm × 1.1 mm CSP package was chosen as the accelerometer, and the fabricated flexible PCB part has a radius of 3 mm. Its acquired micromotion data was transmitted through I^2C interface on flexible wires to Nordic nRF52840, a SoC with Bluetooth module and WLCSP package of 3.5 mm × 3.6 mm and PCB size of 1.1 cm × 1.5 cm. Resistance, inductance or capacitor of 0201 was used for minimization of the whole apparatus. MC3672 has 14-bit resolution, ±16 g range, 1000 Hz sample rate, low noise to 2.3 mgRMS (∼100 Hz), and ∼1 μA typical current, and nRF52840 has Bluetooth 5, ARM Cortex-M4 processor, and advanced on-chip interfaces. The whole system was fabricated by AKM electronics industrial LTD. (Suzhou, Jiangsu, China). Due to the small footprint, light weight, ultralow power consumption, and state-of-the-art flexible PCB, the whole system are thus optimized for wearable HR sensing. The raw acceleration data was transmitted from the accelerometer to the SoC, and to a laptop or desktop. The firmware was developed with μVision 5.28 based on NordicSemi nRF SDK 15.3. The algorithm was demonstrated on MATLAB R2020a in a 64-bit Microsoft Windows-10 Enterprise with Intel Core-i7 CPU (3.7 GHz) and 16-GB RAM. The average computation time for the execution of the proposed algorithm on a 60 s segment is ∼3 s.

Here, 20 healthy subjects, whose ages vary from 23 to 35 (9 males and 11 females) from Southeast University, were recruited by trained staff. All participants provided written informed consent, and the methods were executed according to relevant guidelines and regulations. This study was approved by the institutional review board of Southeast University. Each subject wore the device on the left wrist, with accelerometer on radial artery, and a HR monitor chest strap base on ECG, Polar H10 [7] for reference. During the whole experiments, subjects' left arms were required to keep static, tap fingers or move hands. The movements were instructed to be carried out in large and small amplitudes, high and low frequencies, whereas the exact amplitudes and frequencies were not given and up to the subject. Amplitudes and frequencies variation were considered to include different levels of noise intensity. The two movement patterns we selected are those proven to be the most frequent for continuous HR measurement. For each subject, the data length of experiment is about 10 minutes. Accelerometry data was acquired at 40 Hz, with maximum gain and ±2 g range.

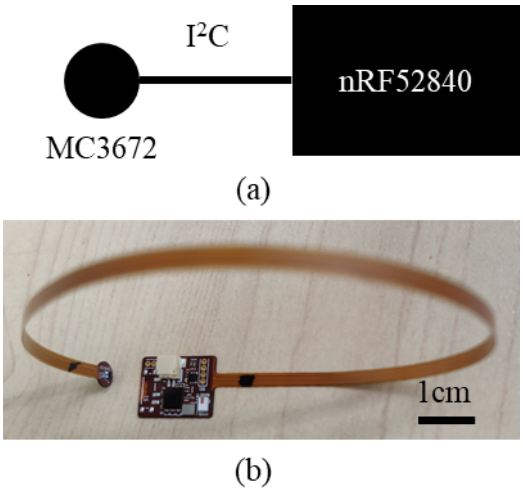

Fig. 1. (a) Design of the heart rate monitor: accelerometer MC3672 communicating with SoC nRF52840 through I^2C protocol, and (b) the fabricated flexible printed circuit device.

B. Decomposition for Automated Motion Artifact and Noise Removal

Typing keyboards or tapping smartphone screen are the most common motion artifacts during office hours or everyday life. Another common motion artifact is hand moving like picking up or laying down cell phones or drinking bottles. An example of the acceleration signals when the subject is static, finger tapping or typing, or hands swing or shaking is presented in Fig. 2. In this subsection, four widely used and popular signal decomposition methods, ICA, VMD, WSST and SSA were implemented and compared. For ICA, RobustICA rather than FastICA was chosen, as it can avoid prewhitening, is robust to local extrema and shows a high convergence speed particularly for short data records [35]. Non-recursive VMD was implemented, not the widely used recursive empirical mode decomposition (EMD), as it is much more robust to sampling and noise [36]. Linear or quadratic time-frequency signal processing and analysis, like Continuous Wavelet

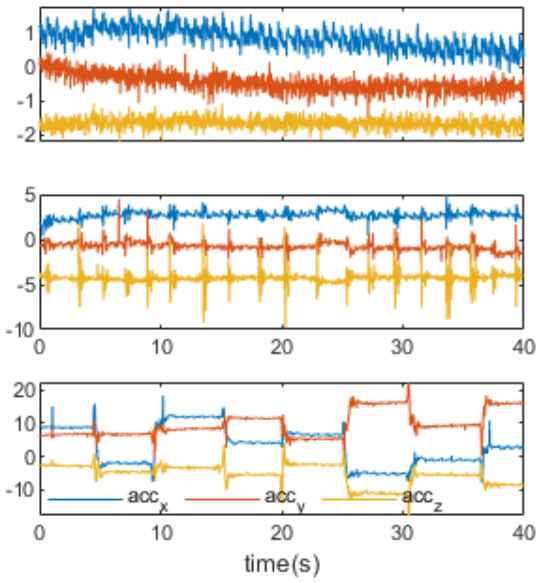

Fig. 2. Top: acceleration signals in 3D when the subject is static. Middle: acceleration signals in 3D when the subject is tapping fingers. Bottom: acceleration signals in 3D when the subject is swinging hands.

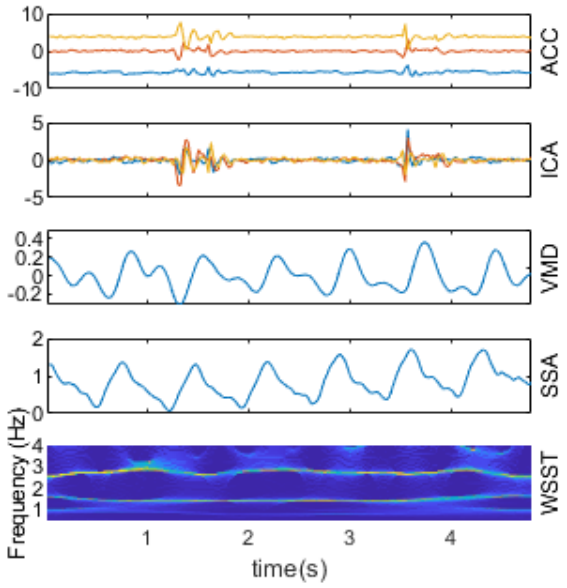

Fig. 3. Acceleration signals in a data segment with finger tapping motions, and its waveform or spectrum reconstructed by ICA, VMD, SSA or WSST.

Transformation (CWT), Short-Time Fourier Transform (STFT) or Wigner-Ville Transform (WVT), suffers from blurred ridge or interferences in the process, and WSST shows sharp ridge with minimized interference [37], [38]. Thus, WSST was selected for spectrum analysis for signal decomposition. For ICA, all 3D accelerations were input as observed signals, and 3 estimated source signals were calculated. For VMD, the number of modes were 7, and the balancing parameter of the data-fidelity constraint was 80 heuristically. For WSST, the analytic Morlet wavelet was used.

For SSA, an observation window of 8 s was employed with 6 s overlapping between consecutive windows, thus a new HR was estimated every 2 s. As the data sampling frequency was set at 40 Hz, each data segment contained 320 data points. The correlation between 3-axis acceleration implies separation of singular vectors of heart beating from motion artifact and noise. A 192×128 Hankel matrix was generated, which yields for decomposition of a matrix

$$\mathrm{D} = \mathrm{U} \Sigma V^T \tag{1}$$

where D is the raw matrix, Σ is the diagonal matrix of singular values in decreasing order, U contains the left singular vectors and V contains the right singular vectors. Decomposed component selection is based on thresholding of eigenvalues and eigenvectors. Different from applying the algorithm on sensors of PPG and accelerometer previously [39], we applied it on 3 axis acceleration of one single accelerometer. The left eigenvector matrices of U_x, U_y and U_z is considered. Without losing generality, we assumed the pulse wave signal is mostly on the x axis, and calculated the principal component by

$$C_{x,y}\,(\mathrm{i}) = \max_{j \in [1,J]} u_x^T\,(i)\, u_y\,(j) \tag{2}$$

where $C_{x,y}\,(\mathrm{i})$ is the ith principal component of x and y axis, J is the total number of eigenvectors, u_x is the eigenvector in U_x and u_y is the eigenvector in U_y. Then a threshold τ is set at 0.6 to differentiate the pulse signal from motion artifact:

$$\max\left(C_{x,y}\,(\mathrm{i})\,, C_{x,z}\,(\mathrm{i})\right) < \tau \tag{3}$$

The eigenvectors obeying the above equation were selected and aligned to form a Σ_{HR}, and to derive an acceleration matrix without motion artifact:

$$\mathrm{D}_{HR} = \mathrm{U} \Sigma_{HR} V^T \tag{4}$$

Fig. 3 and 4 showed the acceleration signals of 3 axes distorted by finger tapping or hand moving motion artifacts respectively, and the reconstructed acceleration by signal decomposition of the above four methods. RobustICA could not handle this type of artifacts, as signals between the HR and finger motion were not statistically independent. VMD and SSA showed promising waveform extracted for HR derivation, while SSA presented better motion artifact removal. For finger motion, WSST showed a clear ridge of HR between 1∼2 Hz, while the spectrum was severely contaminated in the hand motion case. Overall, VMD and SSA were designated as the signal composition method, rather than ICA and WSST. The HR was computed by peak detection with a minimum peak distance constraint after the signal decomposition.

C. Kalman Smoothing

Sensors are noisy, and random motion artifacts corrupting the heart beating signal at the same level as or more than Fig. 3 and Fig. 4 could potentially make the estimated HR deviate further away from the true value even with efficient signal decomposition. For continuous heart rate monitoring, Kalman filter could partially remove the outliers and smooth the time series data by state space methods. Basically, it includes two steps: prediction and update. In the prediction step, *a priori*

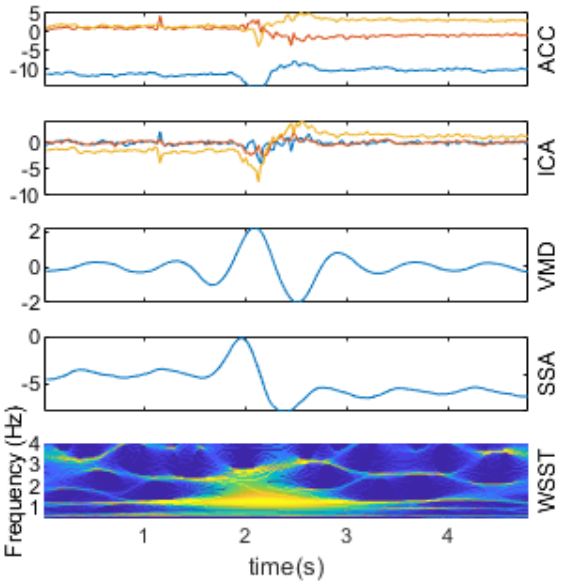

Fig. 4. Acceleration signals in a data segment with hand swinging motions, and its waveform or spectrum reconstructed by ICA, VMD, SSA or WSST.

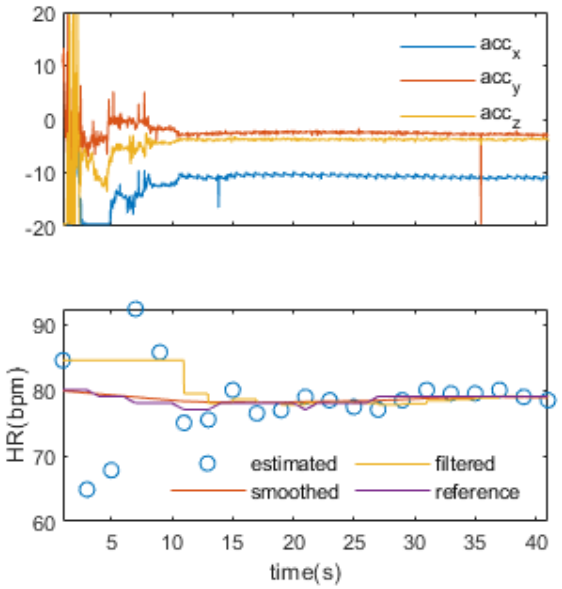

Fig. 5. Kalman filter vs. Kalman smoothing. Top: acceleration signals in 3 axes. It took ∼10 s for the subject to wear the sensor, and then the subject remained static. Bottom: The Kalman filtered result is severely influenced by the initial outliers estimated by SSA, while the Kalman smoothed result correlated much better to the reference.

estimate $\bar{\boldsymbol{x}}, \bar{\boldsymbol{P}}$ is calculated by the model

$$\bar{\boldsymbol{x}} = \boldsymbol{F}\boldsymbol{x} + \boldsymbol{B}\boldsymbol{u} \tag{5}$$

$$\bar{\boldsymbol{P}} = \boldsymbol{F}\boldsymbol{P}\boldsymbol{F}^T + \boldsymbol{Q} \tag{6}$$

where $\boldsymbol{x}, \boldsymbol{P}$ are the state mean and covariance, $\boldsymbol{F}$ is the state transition function, $\boldsymbol{Q}$ is the process covariance, and $\boldsymbol{B}\boldsymbol{u}$ are inputs to the system. Then in the update step, *a posteriori estimate* $\hat{\boldsymbol{x}}, \hat{\boldsymbol{P}}$ is derived by

$$\boldsymbol{y} = \boldsymbol{z} - \boldsymbol{H}\bar{\boldsymbol{x}} \tag{7}$$

$$\boldsymbol{K} = \bar{\boldsymbol{P}}\boldsymbol{H}^T \left(\boldsymbol{H}\bar{\boldsymbol{P}}\boldsymbol{H}^T + \boldsymbol{R}\right)^{-1} \tag{8}$$

$$\hat{\boldsymbol{x}} = \bar{\boldsymbol{x}} + \boldsymbol{K}\boldsymbol{y} \tag{9}$$

$$\hat{\boldsymbol{P}} = (\boldsymbol{I} - \boldsymbol{K}\boldsymbol{H})\,\bar{\boldsymbol{P}} \tag{10}$$

where $\boldsymbol{H}$ is the measurement function, $\boldsymbol{z}$, $\boldsymbol{R}$ are the measurement mean and noise covariance, $\boldsymbol{y}$ is the residual and $\boldsymbol{K}$ is the Kalman gain.

For nonlinear process with non-Gaussian noise, Unscented Kalman Filter, Extended Kalman Filter or Particle Filter are introduced. In our case, Kalman Filter is sufficed to solve the HR tracking problem. Besides Kalman Filter, Kalman Smoothing by utilizing all data before and after current time point could further improve the result [40]. The Rauch-Tung-Striebel (RTS) algorithm is implemented, and the process estimates states going backwards in the time series. Similarly, in the prediction step:

$$\bar{\boldsymbol{P}}_{k+1} = \boldsymbol{F}_k \boldsymbol{P}_k \boldsymbol{F}_k^T + \boldsymbol{Q}_k \tag{11}$$

where the subscript k denote present time point data, and $k+1$ is the following time point. In the update step:

$$\mathbf{K}_k = \hat{\mathbf{P}}_k \boldsymbol{F}_k \bar{\boldsymbol{P}}_{k+1}^{-1} \tag{12}$$

$$\hat{\mathbf{x}}_k^s = \hat{\mathbf{x}}_k + \mathbf{K}_k \left(\hat{\mathbf{x}}_{k+1}^s - \bar{\boldsymbol{x}}_{k+1}\right) \tag{13}$$

$$\hat{\mathbf{P}}_k^s = \hat{\mathbf{P}}_k + \mathbf{K}_k \left(\hat{\boldsymbol{P}}_{k+1}^s - \bar{\mathbf{P}}_{k+1}\right) \mathbf{K}_k^T \tag{14}$$

where $\hat{x}_k^s$ and $\hat{P}_k^s$ are the state mean and covariance of Kalman smoothed estimates. Here, parameters from the next time point were utilized to update the current time point.

Fig. 5 showed an example of comparing Kalman filter and smoother to remove outliers and show matched HR tracking result with the reference method based on ECG. The sensor was worn on the wrist near the radial artery for ∼10 s, and then the hand was kept static for ∼30 s. In the top part of Fig. 5, the raw acceleration signal for the first ∼10 s during the process of wearing the sensor on the wrist caused a severe motion artifact. At the bottom of Fig. 5, heart rate for every 2 s was estimated by SSA in the previous subsection, and Kalman filter and Kalman smoother were implemented to compare the results. HR and Heart Rate Variability (HRV) were selected as the two states. The process covariance was decided by the HR change in the whole monitoring session, and set at a small value as the object was sitting with hand or finger moving, whereas a large process covariance is needed if HR value was influenced by the motion artifact severely. Besides the process model, the sensor measurement noise covariance was set at a value large enough to accommodate HR influenced by the motion artifact, and small enough to remove outliers effectively. For Kalman filter and Kalman smoother, the same sets of parameters were used. Kalman filter showed good result after the starting 10 s as it is a forward pass filtering method, whereas Kalman smoother using RTS proved a much better tracking result since it is applied in a forward-backward manner. The curve of Kalman smoother nearly overlapped with the reference demonstrating its performance. Thus, all following HR tracking was smoothed by Kalman smoother, rather than Kalman filter.

As accelerometer has three-dimensional data, the chosen axis as a principle one is decided by the standard deviation of

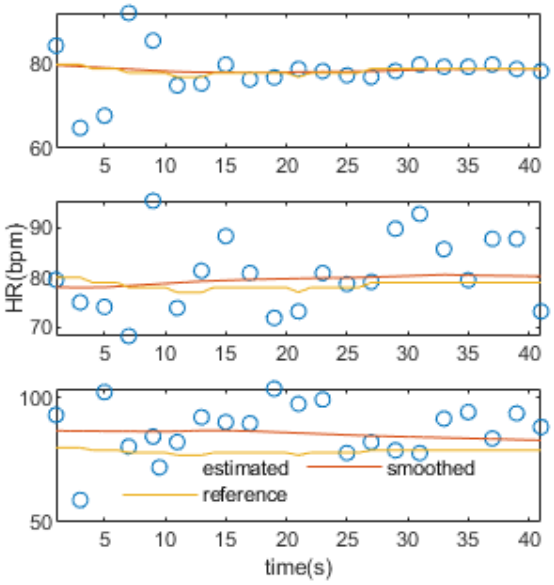

Fig. 6. Choice of principle axis. The principle axis is x axis (top), y axis (middle), and z axis (bottom). In this case, x axis is chosen as the principle axis, because it clearly resulted in the smallest error between HR estimates and Kalman smoothed curve.

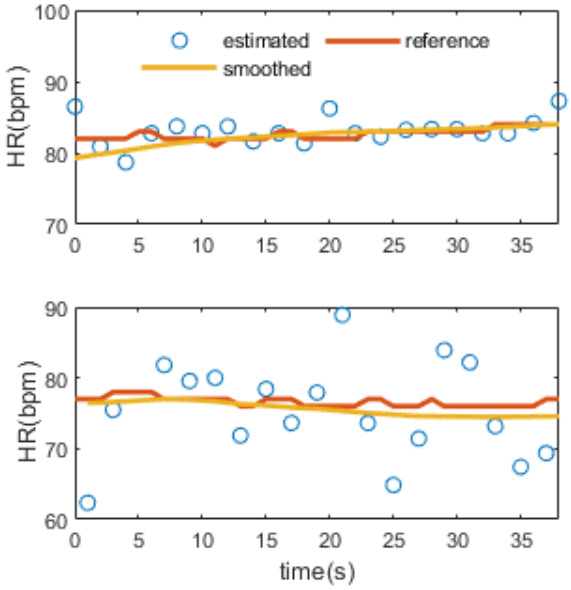

Fig. 7. Effect of finger or hand motions. Top: For finger motions, SSA estimates showed a small SD with reference. Bottom: For hand motions, SSA estimates showed a large SD with reference, and Kalman smoother is a must.

raw HR estimates against the smoothed curve. Fig. 6 showed the smoothing result for 3 axes. Clearly x axis is preferred over y and z in this case.

III. Results

For characterizing the performance of our system, we consider three performance metrics:

1) The average absolute deviation

$$\varepsilon_1 = \frac{1}{N}\sum |HR_{our} - HR_{ECG}| \tag{15}$$

2) The maximum absolute deviation

$$\varepsilon_2 = max\,|HR_{our} - HR_{ECG}| \tag{16}$$

3) The standard deviation

$$\varepsilon_3 = \sqrt{\frac{1}{N}\sum |HR_{our} - HR_{ECG}|^2} \tag{17}$$

where HR_{our} is HR estimates from our system, and HR_{ECG} is the HR reference from ECG.

A. Experiment I: Individual Finger or Hand Motion Within 1 min

We aim to investigate the effectiveness of our method under random finger motions in a short time period first. One object moved random finger at random frequency and force magnitude for 16 times within 40 s, and the 3-axis acceleration data was illustrated in the middle part of Fig. 2. Compared with static posture, it is clear that the finger tapping motions were diverse in the sense of force magnitude and signal waveform. It was illustrated that for finger motions in top part of Fig. 7, the estimation by SSA was closely tracking the true HR with small variations. Whereas by using Kalman smoothing to remove outliers and further smooth raw HR estimates, it enabled the heart rate to be monitored continuously. Statistically, the $\varepsilon_1/\varepsilon_2/\varepsilon_3$ were 1.31/4.49/1.87 for finger motions by SSA, and further decreased to 0.73/2.73/1.04 after Kalman smoothing. Thus, our device and algorithm could monitor heart rate continuously with motion artifact of random finger tapping removed automatically and efficiently.

Then, we intent to demonstrate our methods on detecting heart rate and minimizing motion artifact of random hand motions. In this case, one object wearing the accelerometer on the wrist moved the hands in random directions with random speed magnitude for 8 times within 40 s. Different from finger tapping motion artifact presented with waveform like a distorted wavelet, hand motion resulted in a waveform like a combo of distorted pulse and step function (Fig. 2). The estimated HR using SSA were presented alongside with reference on the bottom of Fig. 7. Estimated HR values were scattering around the reference, making Kalman smoothing critical. Only SSA resulted in $\varepsilon_1/\varepsilon_2/\varepsilon_3$ at 6.17/14.66/7.57 for hand motions, and after Kalman smoothing, the $\varepsilon_1/\varepsilon_2/\varepsilon_3$ dramatically reduced to 1.10/2.45/0.73 for hand motions in Fig. 7.

B. Experiment II: Mixed Hand and Finger Motions Within 1 Hour

After demonstrating our methods for finger tapping/typing or hand swinging/shaking separately in short time segments in Fig. 7, their mixed combo was also tested for 45 min in Fig. 8. These motion artifacts were not rhythmical, and were composed of intermittently random and unpredictable finger or hand motion artifacts. From the acceleration signals, hundreds of motion artifacts were visually identified. In Fig. 8, VMD was firstly utilized to track HR based on only one axis of the accelerometer. On many time segments, motion artifacts

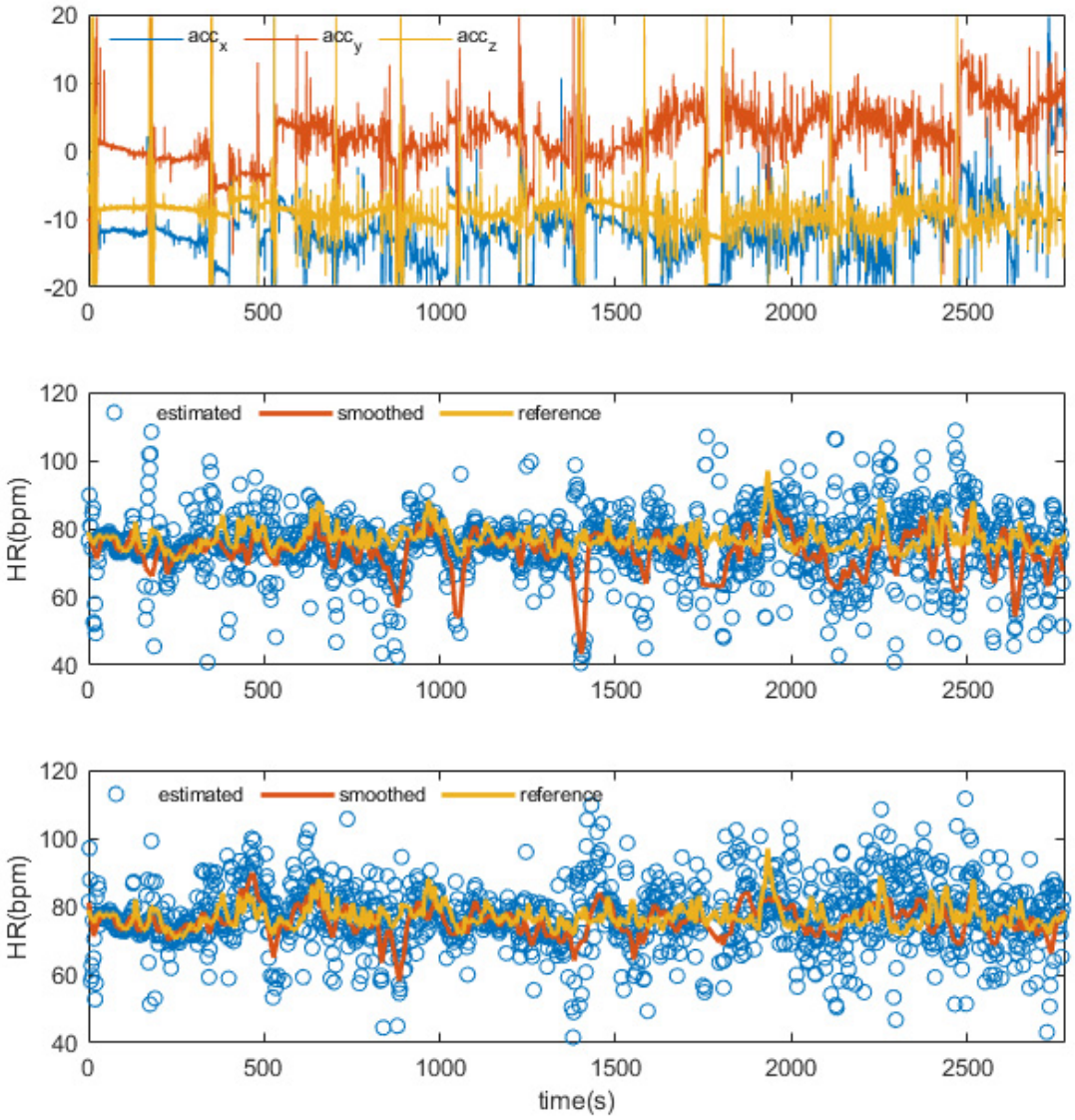

Fig. 8. Continuous monitoring of HR for 45 minutes with motion artifacts removed. Top: Raw acceleration signals in 3D. Middle: The HR estimated by VMD and kalman smoother. Bottom: The HR estimated by SSA and kalman smoother.

severely contaminated the heart rate signal and resulted in many outliers after VMD, that even Kalman smoother was inefficient. By considering all three axis acceleration signals of one sensor, SSA was demonstrated to partially remove motion artifacts and noise shown in Fig. 8. For comparison, $\varepsilon_1/\varepsilon_2/\varepsilon_3$ were estimated at 5.15/33.79/6.12 for VMD and 3.68/18.9/4.52 for SSA. The maximum absolute deviation decreased a lot, meaning more efficient removal of motion artifacts by SSA. The diminishing of average absolute deviation and standard deviation indicates the overall boosted performance of tracking HR by SSA.

Based on the guideline of ANSI/AAMI EC13, for a medical device, the estimated HR is recommended to be within $\pm 10\%$ or ± 5 bpm, whichever is greater. These criteria refer to every individual HR estimation, and is quite difficult to meet for wearable sensors. As shown by the histogram of Fig. 9, by using our method, HR estimation in 93% of the time segments already meets the medical device requirements.

C. Experiment III: Validation on 20 Subjects

Here, 20 healthy subjects (9 males and 11 females) from Southeast University were recruited by trained staff. The age of the participants was 27.5 ± 4.4. Each subject wore the accelerometer on the left wrist, and tapped finger or moved hands for at least 32 times while sitting for 2 minutes. This study was approved by the institutional review board of Southeast University. All participants provided written informed consent, and the methods were executed according to relevant guidelines and regulations. The performance metrics for the proposed system was summarized in Table I. Our novel methods by using SSA on all 3 axis acceleration signals clearly outperformed the VMD on single axis signal, with the $\varepsilon_1/\varepsilon_2/\varepsilon_3$ decreased correspondingly. The standard deviation ε_3' in the table was obtained from Kalman filter, and ε_3 obtained from Kalman smoother clearly outperformed the filter in all subjects. Bland-Altman plot of the HR estimated by VMD and SSA are shown in Fig. 10. As can be seen, VMD had

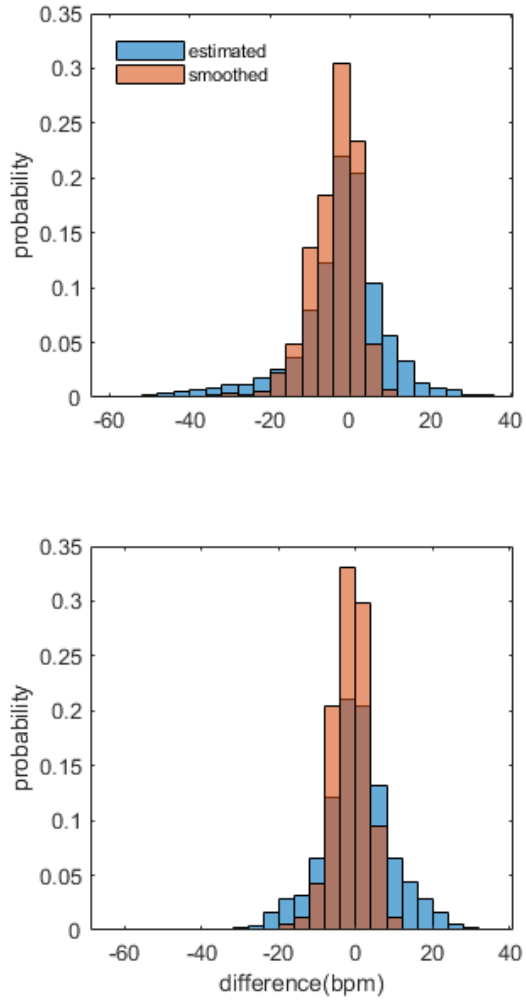

Fig. 9. Deviations of HR estimates and smoothed results from reference values. Top: VMD. Bottom: SSA. For SSA, 93% of the time that the difference meets the medical device requirements, while for VMD, the percentage is 76%.

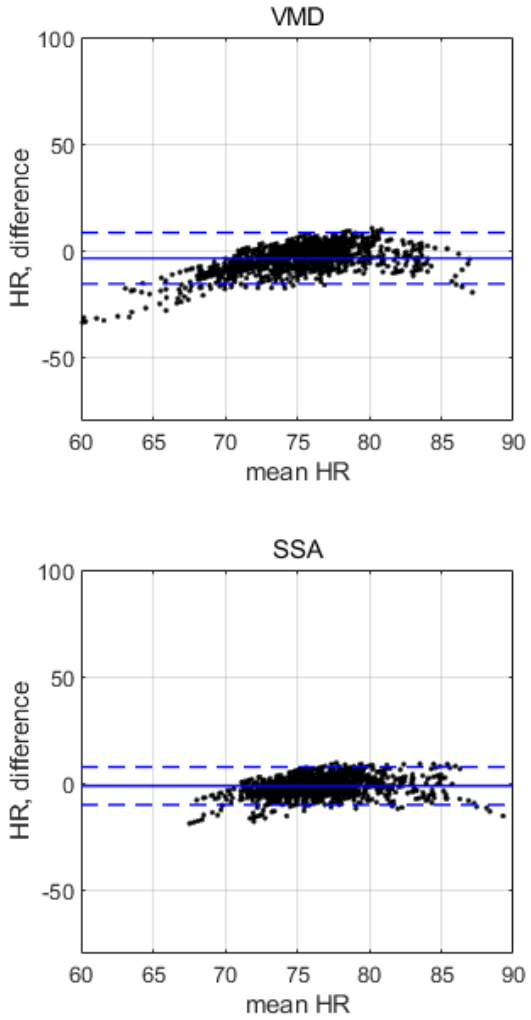

Fig. 10. Bland-Altman plot for the VMD and SSA applied to the 20 subjects with average error and 95%-limits of agreement. VMD had 95% of differences falling within ±12.00 bpm, and SSA had 95% of values within ±8.86 bpm.

95% of differences falling within ±12.00 bpm, and SSA had 95% of values within ±8.86 bpm. Further analysis showed that under those settings when the object is in motion or static, more than 90% of the time, our system already meet the accuracy needed for medical usage based on the guideline of ANSI/AAMI EC13 [7].

IV. Discussion

Accelerometer have not been extensively investigated as a standalone heart rate monitor attached to wrist, because motion artifact on the wrist is complicated, and most of previous work were focused on accelerometers attached to the chest, carotid or superficial temporal artery area. Besides experiments with sensors on the wrist in the previous part, sensors attached to the superficial temporal artery were also tested to prove that our hardware is fit for other exposed skin area (data not shown). Whereas for wearable soft electronic devices, the wrist is the most popular part of the body with inherent end-user appeal. We designed and developed a wrist-worn device and algorithms for measuring heart rate and removing motion artifact all at once based on a single accelerometer. From the aspect of hardware, it's novel as only one sensor is needed. From the aspect of algorithm, it's considering the correlations between all 3 axis acceleration signals, rather than choosing one axis signal and dumping others. Also, no templates of the motion artifacts need to be extracted beforehand, especially considering many motion artifacts are unpredictable. Our framework's innovation lies in the fact that from the time-frequency analysis, heart beating was mainly on one principle axis whereas motion artifact is presented randomly in all directions. Thus, the eigenvectors with high correlation between acceleration on different axes are generally caused by motion artifact, whereas those with low correlation are engendered by heart beating. Without prior knowledge of the motion artifacts, our method could automatically decide which axis should be set as principle axis. Moreover, Kalman smoothing is implemented to derive heart rate with acceptable accuracy, no matter whether the object is static, moving fingers or hands randomly. Compared to other commercial HR monitor, the Apple Watch had 95% of differences falling within −27 bpm and +29 bpm, while Fitbit Charge HR had 95% of values within −34 bpm and +39 bpm, with HR ranging from 49 bpm to 200 bpm [7]. If the HR

TABLE I
PERFORMANCE OF HR ESTIMATION RESULTS FROM 20 HEALTHY SUBJECTS USING VMD AND SSA. (UNIT: BPM)

No.	VMD			SSA			
	ε_1	ε_2	ε_3	ε_1	ε_2	ε_3	ε_3'
1	2.11	6.25	2.51	1.72	6.54	2.06	6.59
2	4.09	13.56	4.38	2.01	6.21	2.35	6.72
3	2.77	9.3	3.07	2.38	9.92	2.98	8.05
4	4.12	14.91	3.59	3.84	9.18	4.57	8.43
5	2.96	10.81	3.27	3.53	8.76	4.25	8.84
6	3.88	9.68	3.58	2.66	7.6	2.98	8.23
7	7.75	20.27	6.82	7.38	18.69	6.92	11.53
8	7.35	19.97	7	3.77	12.42	4.22	14.63
9	2.63	9.68	3.29	2.47	7.29	3	4.3
10	2.53	6.92	3.01	3.76	9.18	2.61	10.48
11	8.28	34.04	11.96	4.78	10.52	5.58	11.74
12	3.96	11.81	4.56	4.4	15.77	5.28	10.07
13	7.77	16.43	5.22	3.62	8.61	2.7	8.45
14	5.05	17.09	5.91	5.12	13.23	5.86	10.38
15	5.41	19.89	6.61	4.33	15.58	5.32	10.1
16	8.34	12.9	2.37	2.42	7.23	2.83	10.61
17	5.06	13.83	5.65	4.49	9.17	4.67	11.18
18	8.13	18.1	8.53	5.5	11.82	5.87	10.86
19	4.01	10.95	4.99	2.6	6.83	3.1	11.43
20	7.23	24.81	7.29	3.14	8.33	2.64	9.16
Avg	**5.17**	**15.06**	**5.18**	**3.70**	**10.14**	**3.99**	**9.59**

were only from 60 bpm to 90 bpm, both of the two existing state-of-the-art had 95% of values within about ± 8 bpm. As a typical PPG module with a footprint of 3.3 mm $\times$ 5.6 mm, like MAX86150 from Maxim Integrated, it required an extra 3.3V for LED besides the normal 1.8V power source, and continuous HR monitoring demanded a constant LED current of 50 mA or 100 mA. This is the reason why most of the commercial HR monitoring by PPG only update HR at interval of tens of seconds or minutes. However, our device achieved 95% of values within ± 8.86 bpm with much lower power consumption (0.9 μA to 36 μA) and smaller footprint (1.3 mm $\times$ 1.1 mm). From the aspect of wearing comfort and nearly 1000 times longer battery life, our device could find more applications and user satisfaction for continuous HR monitoring.

Although in Fig. 2 and Fig. 7, the HR monitored was in a relatively small range ($<$ 10 bpm), as the emphasis is on the hand-related motion artifact removal, a much larger HR range would not invalidate our method. Indeed, even if the HR was fluctuating in a much larger range ($<$ 40 bpm), as the physics behind still works, our system could still track HR efficiently with just larger deviations in Fig. 8, with ε_1 and ε_2 increased by about 2.5 and 3.5 bpm. Thus, even when the HR changed by 80 bpm or more in several minutes, our system could still track HR efficiently. Types of motion artifacts are the main source of uncertainty rather than testers with various gender, age, weight or other physiological profiles. The reported hand motion artifacts are enough to prove the performance is representative.

Nevertheless, several insights and limitations were identified. Firstly, motion artifact with total time segments shorter than or comparable with heart beat is prone to be eliminated by SSA and Kalman smoothing. If there are no time segments that the acceleration signal is dominated by heart beating, such as the hand is moving non-stop that the attachment of the sensor to the skin is compromised, our device could hardly extract clean HR for further smoothing. In ambulatory settings or at home, often there are many time segments with hand relatively static. Thus, SSA could reconstruct the acceleration signal even with some motions, and Kalman smoothing would get a reasonable monitoring results with outliers removed and estimates smoothed. The displacement of sensor to the skin influences the overall performance, which partially caused higher standard deviation in hand motion case in Fig. 7 compared to finger motion case. The measurement system mass was already minimized and the stiffness of the flexible printed circuit was optimized, more friction force needs to take place and an adequate pressure needs to be applied. Secondly, although 99% of the absolute HR differences lie within 5.025 bpm every 2 s[42], setting Kalman process noise covariance this high in our experiments without intense motion artifacts will result in an unacceptable deviations. Hence, we propose that the parameter sets of the Kalman smoother should be able to adjust automatically in the future, unlike constant values here. For example, if the object is doing intense exercise, which could be detected by the accelerometer, a larger process covariance should be assigned to track the changing HR, while the Kalman smoother's sensor noise covariance would be kept constant. Furthermore, more sophisticated Bayesian filter like the Particle Filter method [41], [43], which does not need to assume a specific distribution of the signal or the noise, could be studied to handle more complicated scenarios with the cost of higher computation workload. Thirdly, the main drawback of the proposed method is that cardiac motions are subtle and can be easily occluded by other body motions, like running. Experiments of the subject during walking, jogging, or running showed serious contamination of the HR signal by hand swinging, and further analysis also exposed our system's limitations. Nevertheless, our method provides the possibility of using single wrist-worn accelerometer as a complementary approach in future devices. In a naturalistic real-life environment, our accelerometer could indicate a motion index, and HR during relatively still moments, with motion index below the threshold, are monitored with much smaller power consumption. Beyond the threshold, PPG is needed and a single accelerometer is inadequate, but could be utilized to remove motion artifacts. Overall, our proposed method explored the possible application of accelerometer further on subtle HR signals, compared to capturing large and easily observable motions such as steps, walking and running. In summary, our device is capable of monitoring HR with motion artifacts removed automatically based on only one wrist-worn accelerometer, while future research could focus on sensor attaching methods or other Bayesian filtering algorithms to generate a more robust measurement and sensor models.

V. CONCLUSION

Accelerometers are ubiquitous and could offer low-cost physiological assessments of resting heart rate with much lower power consumption such as a PPG. Our method provides the ability of a single accelerometer on the wrist for HR monitoring. While there are still many challenges, especially the occlusion of HR signals by large and easily observable motions, we have shown it is possible to monitor HR using

low-cost and energy-efficient motion sensors with motion artifacts and noise removed automatically during relatively still moments, which could make HR assessments more frequent and widely available.

REFERENCES

[1] K. Fox *et al.*, "Resting heart rate in cardiovascular disease," *J. Amer. College Cardiol.*, vol. 50, no. 9, pp. 823–830, 2007.

[2] A. Lanata, G. Valenza, M. Nardelli, C. Gentili, and E. P. Scilingo, "Complexity index from a personalized wearable monitoring system for assessing remission in mental health," *IEEE J. Biomed. Health Informat.*, vol. 19, no. 1, pp. 132–139, Jan. 2015.

[3] S. S. Thomas, V. Nathan, C. Zong, K. Soundarapandian, X. Shi, and R. Jafari, "BioWatch: A noninvasive wrist-based blood pressure monitor that incorporates training techniques for posture and subject variability," *IEEE J. Biomed. Health Informat.*, vol. 20, no. 5, pp. 1291–1300, Sep. 2016.

[4] A. M. Carek, J. Conant, A. Joshi, H. Kang, and O. T. Inan, "SeismoWatch: Wearable cuffless blood pressure monitoring using pulse transit time," *Proc. ACM Interact., Mobile, Wearable Ubiquitous Technol.*, vol. 1, no. 3, pp. 1–16, Sep. 2017.

[5] J. Allen, "Photoplethysmography and its application in clinical physiological measurement," *Physiolog. Meas.*, vol. 28, no. 3, pp. R1–R39, Mar. 2007.

[6] C. Holz and E. J. Wang, "Glabella: Continuously sensing blood pressure behavior using an unobtrusive wearable device," *Proc. ACM Interact., Mobile, Wearable Ubiquitous Technol.*, vol. 1, no. 3, pp. 1–23, Sep. 2017.

[7] R. Wang *et al.*, "Accuracy of wrist-worn heart rate monitors," *JAMA Cardiol.*, vol. 2, no. 1, pp. 104–106, 2017.

[8] Z. Zhang, "Photoplethysmography-based heart rate monitoring in physical activities via joint sparse spectrum reconstruction," *IEEE Trans. Biomed. Eng.*, vol. 62, no. 8, pp. 1902–1910, Aug. 2015.

[9] T. H. Huynh, R. Jafari, and W.-Y. Chung, "Noninvasive cuffless blood pressure estimation using pulse transit time and impedance plethysmography," *IEEE Trans. Biomed. Eng.*, vol. 66, no. 4, pp. 967–976, Apr. 2019.

[10] F. Miao, Z.-D. Liu, J.-K. Liu, B. Wen, Q.-Y. He, and Y. Li, "Multi-sensor fusion approach for cuff-less blood pressure measurement," *IEEE J. Biomed. Health Informat.*, vol. 24, no. 1, pp. 79–91, Jan. 2020.

[11] M. Altini, P. Casale, J. F. Penders, and O. Amft, "Personalization of energy expenditure estimation in free living using topic models," *IEEE J. Biomed. Health Informat.*, vol. 19, no. 5, pp. 1577–1586, Sep. 2015.

[12] B. Cvetkovic, R. Milic, and M. Lustrek, "Estimating energy expenditure with multiple models using different wearable sensors," *IEEE J. Biomed. Health Informat.*, vol. 20, no. 4, pp. 1081–1087, Jul. 2016.

[13] M. R. Nelson, J. Stepanek, M. Cevette, M. Covalciuc, R. T. Hurst, and A. J. Tajik, "Noninvasive measurement of central vascular pressures with arterial tonometry: Clinical revival of the pulse pressure waveform?" *Mayo Clinic Proc.*, vol. 85, no. 5, pp. 460–472, May 2010.

[14] N. Di Lascio *et al.*, "Noninvasive assessment of carotid pulse pressure values: An accelerometric-based approach," *IEEE Trans. Biomed. Eng.*, vol. 63, no. 4, pp. 869–875, Apr. 2016.

[15] Q. Zhang *et al.*, "Technology development for simultaneous wearable monitoring of cerebral hemodynamics and blood pressure," *IEEE J. Biomed. Health Informat.*, vol. 23, no. 5, pp. 1952–1963, Sep. 2019.

[16] B. Ma, C. Xu, J. Chi, J. Chen, C. Zhao, and H. Liu, "A versatile approach for direct patterning of liquid metal using magnetic field," *Adv. Funct. Mater.*, vol. 29, no. 28, Jul. 2019, Art. no. 1901370.

[17] C. Xu, B. Ma, S. Yuan, C. Zhao, and H. Liu, "High-resolution patterning of liquid metal on hydrogel for flexible, stretchable, and self-healing electronics," *Adv. Electron. Mater.*, vol. 6, no. 1, pp. 1–8, 2020.

[18] M. J. Tadi *et al.*, "A real-time approach for heart rate monitoring using a Hilbert transform in seismocardiograms," *Physiolog. Meas.*, vol. 37, no. 11, pp. 1885–1909, Nov. 2016.

[19] J. Wahlstrom *et al.*, "A hidden Markov model for seismocardiography," *IEEE Trans. Biomed. Eng.*, vol. 64, no. 10, pp. 2361–2372, Oct. 2017.

[20] T. Choudhary, M. K. Bhuyan, and L. N. Sharma, "A novel method for aortic valve opening phase detection using SCG signal," *IEEE Sensors J.*, vol. 20, no. 2, pp. 899–908, Jan. 2020.

[21] T. Choudhary, L. N. Sharma, and M. K. Bhuyan, "Automatic detection of aortic valve opening using seismocardiography in healthy individuals," *IEEE J. Biomed. Health Informat.*, vol. 23, no. 3, pp. 1032–1040, May 2019.

[22] F. Khosrow-Khavar, K. Tavakolian, A. Blaber, and C. Menon, "Automatic and robust delineation of the fiducial points of the seismocardiogram signal for noninvasive estimation of cardiac time intervals," *IEEE Trans. Biomed. Eng.*, vol. 64, no. 8, pp. 1701–1710, Aug. 2017.

[23] T. Hurnanen *et al.*, "Automated detection of atrial fibrillation based on time–frequency analysis of seismocardiograms," *IEEE J. Biomed. Health Informat.*, vol. 21, no. 5, pp. 1233–1241, Sep. 2017.

[24] M. Paukkunen *et al.*, "Beat-by-beat quantification of cardiac cycle events detected from three-dimensional precordial acceleration signals," *IEEE J. Biomed. Health Informat.*, vol. 20, no. 2, pp. 435–439, Mar. 2016.

[25] G. Karacocuk *et al.*, "Inertial sensor-based respiration analysis," *IEEE Trans. Instrum. Meas.*, vol. 68, no. 11, pp. 4268–4275, Nov. 2019.

[26] D. Jarchi, S. J. Rodgers, L. Tarassenko, and D. A. Clifton, "Accelerometry-based estimation of respiratory rate for post-intensive care patient monitoring," *IEEE Sensors J.*, vol. 18, no. 12, pp. 4981–4989, Jun. 2018.

[27] A. Siqueira, A. F. Spirandeli, R. Moraes, and V. Zarzoso, "Respiratory waveform estimation from multiple accelerometers: An optimal sensor number and placement analysis," *IEEE J. Biomed. Health Informat.*, vol. 23, no. 4, pp. 1507–1515, Jul. 2019.

[28] V. Zakeri, A. Akhbardeh, N. Alamdari, R. Fazel-Rezai, M. Paukkunen, and K. Tavakolian, "Analyzing seismocardiogram cycles to identify the respiratory phases," *IEEE Trans. Biomed. Eng.*, vol. 64, no. 8, pp. 1786–1792, Aug. 2017.

[29] M. Janidarmian, A. R. Fekr, K. Radecka, and Z. Zilic, "Multi-objective hierarchical classification using wearable sensors in a health application," *IEEE Sensors J.*, vol. 17, no. 5, pp. 1421–1433, Mar. 2017.

[30] A. Q. Javaid *et al.*, "Quantifying and reducing motion artifacts in wearable seismocardiogram measurements during walking to assess left ventricular health," *IEEE Trans. Biomed. Eng.*, vol. 64, no. 6, pp. 1277–1286, Jun. 2017.

[31] H. Lee, H. Chung, J.-W. Kim, and J. Lee, "Motion artifact identification and removal from wearable reflectance photoplethysmography using piezoelectric transducer," *IEEE Sensors J.*, vol. 19, no. 10, pp. 3861–3870, May 2019.

[32] T. Chen and C. Guestrin, "XGBoost: A scalable tree boosting system," in *Proc. 22nd ACM SIGKDD Int. Conf. Knowl. Discovery Data Mining*, vols. 13–17, Aug. 2016, pp. 785–794.

[33] W. He, Y. Ye, L. Lu, Y. Cheng, Y. Li, and Z. Wang, "Robust heart rate monitoring for quasi-periodic motions by wrist-type PPG signals," *IEEE J. Biomed. Health Informat.*, vol. 24, no. 3, pp. 636–648, Mar. 2020.

[34] J. Zia, J. Kimball, S. Hersek, M. M. H. Shandhi, B. Semiz, and O. T. Inan, "A unified framework for quality indexing and classification of seismocardiogram signals," *IEEE J. Biomed. Health Informat.*, vol. 24, no. 4, pp. 1080–1092, Apr. 2020.

[35] V. Zarzoso and P. Comon, "Robust independent component analysis by iterative maximization of the kurtosis contrast with algebraic optimal step size," *IEEE Trans. Neural Netw.*, vol. 21, no. 2, pp. 248–261, Feb. 2010.

[36] K. Dragomiretskiy and D. Zosso, "Variational mode decomposition," *IEEE Trans. Signal Process.*, vol. 62, no. 3, pp. 531–544, Feb. 2014.

[37] I. Daubechies, J. Lu, and H.-T. Wu, "Synchrosqueezed wavelet transforms: An empirical mode decomposition-like tool," *Appl. Comput. Harmon. Anal.*, vol. 30, no. 2, pp. 243–261, Mar. 2011.

[38] G. Thakur, E. Brevdo, N. S. Fučkar, and H.-T. Wu, "The synchrosqueezing algorithm for time-varying spectral analysis: Robustness properties and new paleoclimate applications," *Signal Process.*, vol. 93, no. 5, pp. 1079–1094, May 2013.

[39] A. Galli, C. Narduzzi, and G. Giorgi, "Measuring heart rate during physical exercise by subspace decomposition and Kalman smoothing," *IEEE Trans. Instrum. Meas.*, vol. 67, no. 5, pp. 1102–1110, May 2018.

[40] O. M. Staal, S. Salid, A. Fougner, and O. Stavdahl, "Kalman smoothing for objective and automatic preprocessing of glucose data," *IEEE J. Biomed. Health Informat.*, vol. 23, no. 1, pp. 218–226, Jan. 2019.

[41] K. Xu, X. Jiang, S. Lin, C. Dai, and W. Chen, "Stochastic modeling based nonlinear Bayesian filtering for photoplethysmography denoising in wearable devices," *IEEE Trans. Ind. Informat.*, vol. 16, no. 11, pp. 7219–7230, Nov. 2020.

[42] H. Chung, H. Lee, and J. Lee, "Finite state machine framework for instantaneous heart rate validation using wearable photoplethysmography during intensive exercise," *IEEE J. Biomed. Health Informat.*, vol. 23, no. 4, pp. 1595–1606, Jul. 2019.

[43] V. Nathan and R. Jafari, "Particle filtering and sensor fusion for robust heart rate monitoring using wearable sensors," *IEEE J. Biomed. Health Informat.*, vol. 22, no. 6, pp. 1834–1846, Nov. 2018.